

Gravitational waves from a dilaton-induced, first-order QCD phase transition

Aleksandr Chatrchyan,^{1,2,*} M.C. David Marsh,^{1,†} and Charalampos Nikolis^{1,‡}

¹*The Oskar Klein Centre for Cosmoparticle Physics, Department of Physics,
Stockholm University, AlbaNova, 10691 Stockholm, Sweden*

²*Nordita, KTH Royal Institute of Technology and Stockholm University
Hannes Alfvéns väg 12, SE-106 91 Stockholm, Sweden*

(Dated: July 11, 2025)

We show that a ‘QCD dilaton’ field, whose vacuum expectation value sets the strong coupling, can render the Quantum Chromodynamic (QCD) confinement transition first-order. The QCD dilaton is cosmologically attracted to a false vacuum at weak coupling in the early universe. Quantum tunnelling towards the true vacuum triggers prompt chiral symmetry breaking and confinement of QCD, leading to detonating bubbles of the hadronic phase. We find that plasma sound waves produced by this dilaton-induced, first-order QCD phase transition generate a stochastic gravitational wave signal strikingly similar to the recently detected gravitational wave background from Pulsar Timing Arrays. We briefly comment on how this theory can be probed through collider experiments and cosmology.

Despite decades of enormous progress in observational and theoretical cosmology, the first microsecond of the Universe remains poorly known. Direct evidence for events taking place prior to Big Bang Nucleosynthesis (BBN) is scarce, which limits the ability to use cosmology as a ‘poor man’s accelerator’ [1, 2]. The gateway to higher energies is provided by the Quantum Chromodynamic (QCD) phase transition (PT), in which the hot Big Bang plasma transitioned from the high-temperature quark-gluon phase into the low-temperature confined, hadronic phase. In the Standard Model (SM) of particle physics, the QCD PT is a smooth cross-over occurring at temperatures around $T_{\text{QCD}} \sim 160$ MeV [3]. Cross-overs are comparatively calm cosmic events, leaving few observational imprints. Thus, in the SM, the prospects for directly probing the QCD PT are dim.

The QCD confinement PT is accompanied by chiral symmetry breaking and the growth of the strong coupling constant, g_3 . In the Standard Model, g_3 is perturbatively small at high energies and runs to strong coupling at around the QCD scale, which through dimensional transmutation is given by

$$\Lambda_{\text{QCD}} = \mu \exp \left[-\frac{8\pi^2}{\beta_0 g_3^2(\mu)} \right], \quad (1)$$

at one-loop order, where μ is an energy scale, $\beta_0 = 11 - \frac{2}{3}N_f$ for N_f flavours. The ultraviolet value of the coupling constant, $g_3^{\text{UV}} = g_3(\mu_{\text{UV}})$, is, like all Standard Model parameters, assumed to be constant: once fixed, it is unchanging over cosmic time.

By contrast, quantum gravity is expected to have no free parameters or true constants. All parameters of low-energy effective theories, like the Standard Model, are expected to be secretly field-dependent. We refer to the scalar field, $\phi(x)$, that makes the strong coupling constant dynamical as the ‘QCD dilaton’ (or just dilaton, for short).

In this paper, we show that the dynamics of ϕ can ef-

fectively turn the QCD phase transition first-order, leading to detonating bubbles of the confined phase, separated from the quark-gluon plasma by a dilaton domain wall. The expanding bubbles quickly reach relativistic speeds and produce a stochastic gravitational wave background with an amplitude and spectrum that agree well with recent observations from Pulsar Timing Arrays [4–7], thus begging the question: *Have we already observed the first signals from a dilaton-induced first-order QCD phase transition?*

QCD and its dilaton — The Lagrangian of QCD and its dilaton, ϕ , is given by

$$\mathcal{L} = -\frac{1}{2} \mathfrak{f}(\phi) \text{tr}(G_{\mu\nu} G^{\mu\nu}) + \sum_i \bar{q}_i (i \not{D} - m_i) q_i + \frac{1}{2} (\partial\phi)^2 - V_0(\phi), \quad (2)$$

where $G_{\mu\nu} = \partial_\mu A_\nu - \partial_\nu A_\mu - i[A_\mu, A_\nu]$, q_i denotes quark species i , and $\not{D} = \gamma^\mu (\partial_\mu - iA_\mu)$ for the non-Abelian gauge potential, A_μ . The real-valued gauge kinetic function $\mathfrak{f}(\phi)$ sets the QCD coupling constant as $\mathfrak{f}(\langle\phi\rangle) = 1/(g_3^{\text{UV}})^2$ at some high energy scale.

We assume that the zero-temperature dilaton potential, $V_0(\phi)$, has two minima: the true vacuum at ϕ_{TV} and the false vacuum at ϕ_{FV} , with $\Delta V = V_0(\phi_{\text{FV}}) - V_0(\phi_{\text{TV}}) > 0$, and, importantly, $\Delta \mathfrak{f} = \mathfrak{f}(\phi_{\text{FV}}) - \mathfrak{f}(\phi_{\text{TV}}) > 0$. This assumption means that QCD is more weakly coupled in the false vacuum than in the true vacuum. We do not model the microphysical origins of $V_0(\phi)$ and $\mathfrak{f}(\phi)$. In potential string theory realisations of our scenario, ϕ would be a modulus field whose potential can be quite complex, receiving both perturbative and non-perturbative contributions [8–10]. Similarly, the gauge kinetic function may descend from the holomorphic gauge kinetic function of supergravity, which receives both one-loop and non-perturbative corrections [11, 12]. We provide a concrete toy model realising our scenario below, however, many generalisations are possible. Recent work

on related theories include [13–20].

In the present universe, $\phi = \phi_{\text{TV}}$, and the properties of the dilaton are experimentally constrained. The dilaton mass is required to be sufficiently large to avoid collider constraints [21]: $m_{\phi\text{TV}} \gtrsim 5 \text{ TeV}$, under some assumptions on the form of \mathbf{f} . In this work, we assume $m_{\phi\text{TV}} \sim m_{\phi\text{FV}} \sim 10 \text{ TeV}$, for simplicity. Moreover, the QCD coupling constant is set by experiments to $\alpha_s(m_Z^2) = 0.1180 \pm 0.0009$ (cf. [22] and references therein), which implies

$$\mathbf{f}_{\text{TV}} \equiv \mathbf{f}(\phi_{\text{TV}}) = \frac{\beta_0}{8\pi^2} \ln \left(\frac{\Lambda_{\text{UV}}}{m_Z} \right) + \frac{1}{4\pi\alpha_s(m_Z)}.$$

For example, a UV-scale of $\Lambda_{\text{UV}} \sim 10^{19} \text{ GeV}$, implies $\mathbf{f}_{\text{TV}} \simeq 4.2$ for $\beta_0 = 7$ (as appropriate for 6 quark flavours).

The dilaton-dependent QCD scale — The weaker gauge coupling in the false vacuum implies an exponentially lower strong-coupling scale, Λ_{QCD} , than in standard QCD:

$$\Lambda_{\text{QCD}}^{\text{FV}} = \Lambda_{\text{QCD}}^{\text{TV}} \exp \left(-\frac{8\pi^2 \Delta \mathbf{f}}{\beta_0} \right). \quad (3)$$

For $\Delta \mathbf{f} \sim \mathcal{O}(1)$, QCD with $\phi = \phi_{\text{FV}}$ remains weakly coupled well below the Standard Model cross-over temperature $T_{\text{QCD}}^{\text{TV}}$, suggesting that chiral symmetry breaking and confinement would only happen at $T_{\text{QCD}}^{\text{FV}} \ll T_{\text{QCD}}^{\text{TV}}$.

Below the confinement temperature (for any ϕ), we model the low-energy QCD dynamics with a two-quark linear sigma model featuring an explicit chiral symmetry breaking [23]

$$V_\chi(\phi, \chi) = \frac{\lambda}{4} (\chi^4 - 2f_\pi^2 \chi^2) - m_\pi^2 f_\pi \chi, \quad (4)$$

with χ the chiral condensate and $f_\pi(\phi)$, $m_\pi(\phi)$ the pion decay constant and the pion mass, respectively. The quantities f_π , m_π inherit their ϕ -dependence from their dependence on the confinement scale, and obey the scaling relations (cf. [16] for a similar discussion)

$$\frac{f_\pi(\phi_{\text{FV}})}{f_\pi(\phi_{\text{TV}})} = \frac{m_\pi(\phi_{\text{FV}})}{m_\pi(\phi_{\text{TV}})} = \exp \left[-\frac{8\pi^2 \Delta \mathbf{f}}{\beta_0} \right]. \quad (5)$$

Note that, in (4), we have omitted a χ -independent (but ϕ -dependent) contribution $\sim f_\pi^4$, as this contribution can be absorbed into $V_0(\phi)$. Taking $\lambda = 20$ reproduces the condensate mass of $m_\chi = 600 \text{ MeV}$ [24].

More elaborate effective theories modelling the confinement transition in addition to the chiral symmetry breaking can be constructed [25, 26]; however, the simpler linear sigma model suffices to capture the relevant physics of our scenario, which we now discuss.

A dilaton-induced, first-order QCD phase transition — Early in cosmic history, the dilaton was in thermal equilibrium with the quark-gluon plasma and its

dynamics was governed by the temperature-dependent effective potential

$$V_{\text{eff}}(\phi) = V_0(\phi) + V_{\text{T}}(\phi) + V_{\mathcal{P}}(\phi), \quad (6)$$

where

$$V_{\text{T}}(\phi) = \frac{T^4}{2\pi^2} J_{\text{B}} \left(\frac{m_\phi^2(\phi)}{T^2} \right)$$

denotes the one-loop thermal effective potential due to dilaton self-interactions [27]. Here J_{B} is the thermal bosonic function and $m_\phi(\phi)$ is the field-dependent mass. The term $V_{\mathcal{P}}(\phi)$ represents the thermal QCD pressure-corrections ($\mathcal{P}_{\text{QCD}} = -V_{\mathcal{P}}$) in a fixed dilaton background [28]:

$$V_{\mathcal{P}}(\phi) = -\frac{8\pi^2 T^4}{45} \left(\frac{17}{3} - \frac{235}{16} \alpha_s(\phi) + \mathcal{O}(\alpha_s^{3/2}) \right),$$

where $\alpha_s(\phi) = 1/(4\pi\mathbf{f}(\phi))$ [29], [30].

The effective potential of Eq. (6) is shown schematically in the left panel of Fig. 1 for four different temperatures. At sufficiently high temperatures ($T \gg m_\phi$), V_{eff} is dominated by the stabilising, leading-order contribution from V_{T} , $\sim m^2(\phi)T^2$, and the loop-corrected part of $V_{\mathcal{P}}$, which push the dilaton towards weak coupling (corresponding to larger field values). The potential has a single minimum in the range $\phi_{\text{TV}} < \phi < \phi_{\text{FV}}$, slightly offset towards ϕ_{FV} .

At intermediate temperatures, the thermal contributions from self-interactions become Boltzmann-suppressed and can be ignored, and V_{eff} develops a second minimum at smaller field values. Notably, due to $V_{\mathcal{P}}$, the large-field minimum approaching ϕ_{FV} is the global minimum of V_{eff} at these temperatures, and the dilaton is attracted to the false vacuum.

At sufficiently low temperatures, V_{eff} becomes dominated by the zero-temperature potential $V_0(\phi)$, and ϕ_{TV} becomes the new global minimum of the potential. However, the dilaton remains classically trapped at ϕ_{FV} . The right panel of Fig. (1) shows a schematic representation of the full two-field potential, $V_{\text{tot}}(\phi, \chi) = V_{\text{eff}}(\phi) + V_\chi(\phi, \chi)$, for $T_{\text{QCD}}^{\text{FV}} < T < T_{\text{QCD}}^{\text{TV}}$. For $\langle \phi \rangle = \phi_{\text{TV}}$, chiral symmetry is broken by $\langle \chi \rangle \neq 0$ in the vacuum. For $\langle \phi \rangle = \phi_{\text{FV}}$, QCD is in the unconfined phase, and, consistently, $\langle \chi \rangle = 0$ and chiral symmetry is unbroken.

With ϕ in the false vacuum, the quark-gluon plasma may cool below $T_{\text{QCD}}^{\text{TV}}$ without triggering the cross-over transition to the hadron gas (which for $\phi = \phi_{\text{FV}}$ would happen around $T_{\text{QCD}}^{\text{FV}}$). However, the dilaton vacuum is non-perturbatively unstable and eventually decays to ϕ_{TV} through quantum tunnelling, proceeding through the nucleation of true-vacuum bubbles. The nucleation rate per unit volume is given by $\Gamma/\mathcal{V} = Ae^{-S_4}$ [31, 32], with S_4 the time independent $O(4)$ symmetric bounce action, and A a prefactor. We assume that the nucleation

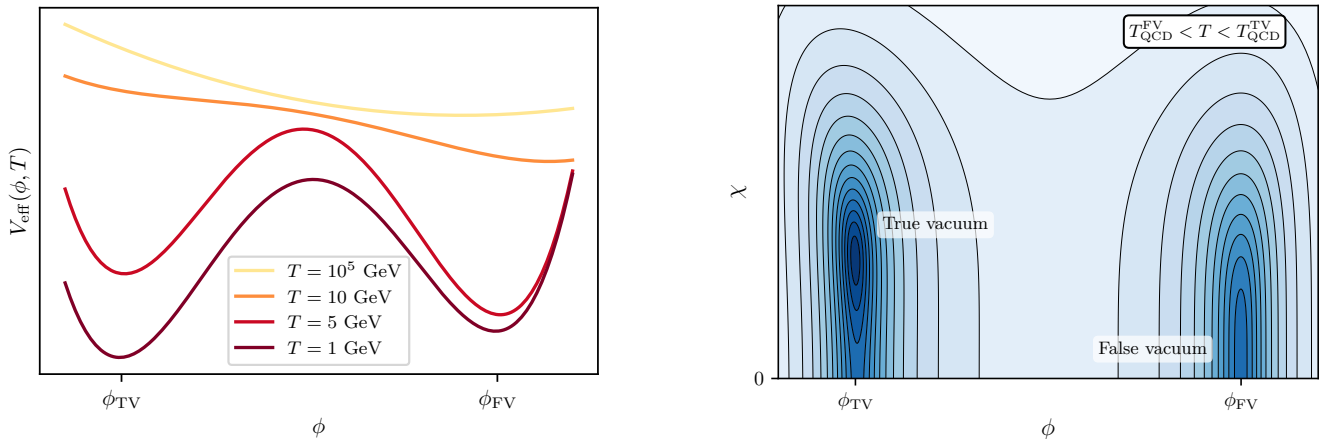


FIG. 1. **Left:** The dilaton potential, $V_{\text{eff}}(\phi)$, at different temperatures. The values of the potential are rescaled for visual clarity. For $T \sim 100 \text{ TeV} \gg m_\phi$ the minimum is located in between the tree-level vacua. As temperature drops ($T \sim \mathcal{O}(10) \text{ GeV} \ll m_\phi$), the minimum moves towards the ϕ_{FV} while a local minimum emerges near ϕ_{TV} . When temperature corrections become unimportant, ϕ_{TV} becomes the global minimum. **Right:** Schematic contour plot for the two-field potential, $V_{\text{tot}}(\chi, \phi)$ for $T_{\text{QCD}}^{\text{FV}} < T < T_{\text{QCD}}^{\text{TV}}$.

temperature, T_n , is in the range

$$T_{\text{QCD}}^{\text{FV}} < T_n < T_{\text{QCD}}^{\text{TV}}, \quad (7)$$

and that $T_n \gtrsim T_{\text{BBN}} \approx 6 \text{ MeV}$ [33]. Fixing the nucleation temperature corresponds to fixing the decay rate through the approximate equation $\Gamma/\mathcal{V} \simeq H^4(T_n)$, expressing that, at T_n , one bubble is nucleated per Hubble volume and Hubble time.

Outside the bubbles, the plasma remains in the pre-confined quark-gluon phase (as $T_n > T_{\text{QCD}}^{\text{FV}}$), but *inside* the bubbles, the temperature is lower than the local QCD confinement scale (i.e. $T_{\text{QCD}}^{\text{TV}}$), leading to prompt hadronisation and chiral symmetry breaking. In the two quark linear sigma model, the approximate timescale of confinement can be found from $t_{\text{roll}} \sim \mathcal{O}(1/m_\chi) \ll H^{-1}$, with $m_\chi = \sqrt{2}\lambda f_\pi$, so chiral-symmetry breaking inside the true-dilaton-vacuum bubbles is approximately instantaneous. Thus, in this scenario, the QCD PT is no longer a smooth cross-over, but characterised by expanding bubbles of the hadronic phase inside the quark-gluon plasma; *this scenario effectively turns the QCD phase transition first order.*

We require that the transition percolates (at plasma temperature T_\star) which, for a PT with constant Γ , requires $\alpha \lesssim 20$ [34], where $\alpha = \Delta V/\rho_{\text{rad}}(T_n)$. For such transitions, the inverse duration of the PT, β , is set by α and satisfies $8 \gtrsim \beta/H_\star > 3$ [34]. As the energy density ΔV is channelled into the Standard Model, the plasma is reheated to the temperature $T_{\text{rh}} = (1+\alpha)^{1/4}T_n$, here assuming $T_\star \approx T_n$. We restrict our discussion to $T_{\text{rh}} \lesssim T_{\text{QCD}}^{\text{TV}}$, so that the hadrons do not deconfine (and then undergo a ‘second’ QCD transition, this time a cross-over).

The subsequent cosmology and observational predictions of this scenario depend on the speed at which the bubbles expand. As we show in the Supplementary Material [35], the bubble walls reach ultrarelativistic terminal velocities before bubbles collide.

Gravitational wave signal — As the relativistic dilaton bubbles grow large, collide, and percolate, they produce a stochastic gravitational wave (GW) background, potentially observable today [36, 37]. This is particularly interesting given the recent observation of the Hellings-Down correlation in Pulsar Timing Array (PTA) datasets [4–7], providing evidence for a stochastic GW background in the nanohertz range. Such a background could potentially be explained astrophysically through supermassive black hole binary mergers [38], but this explanation has difficulties with accommodating the observed amplitude and spectrum [39, 40]. By contrast, several studies have found that GWs generated by a first-order PT provides a better fit to the data [41–55] (see [56] for an alternative gravitational wave explanation generated by turbulent sources regardless of the order of the QCD PT).

Since the bubbles are expected to reach a terminal velocity before they collide, the main contribution to the GW signal in this scenario is from the dynamics of sound waves generated in the plasma [57–61] (the contribution to the signal coming from bubble wall collisions, which is relevant for runaway PTs, is discussed in the Supplementary Material [35]).

Estimates of the amplitude and spectrum of the GW background can be parametrised through rather simple formulas, depending on $T_\star \approx T_n$, α , β , and v_w (cf. [62] and, for a recent review, [63]). The peak frequency is

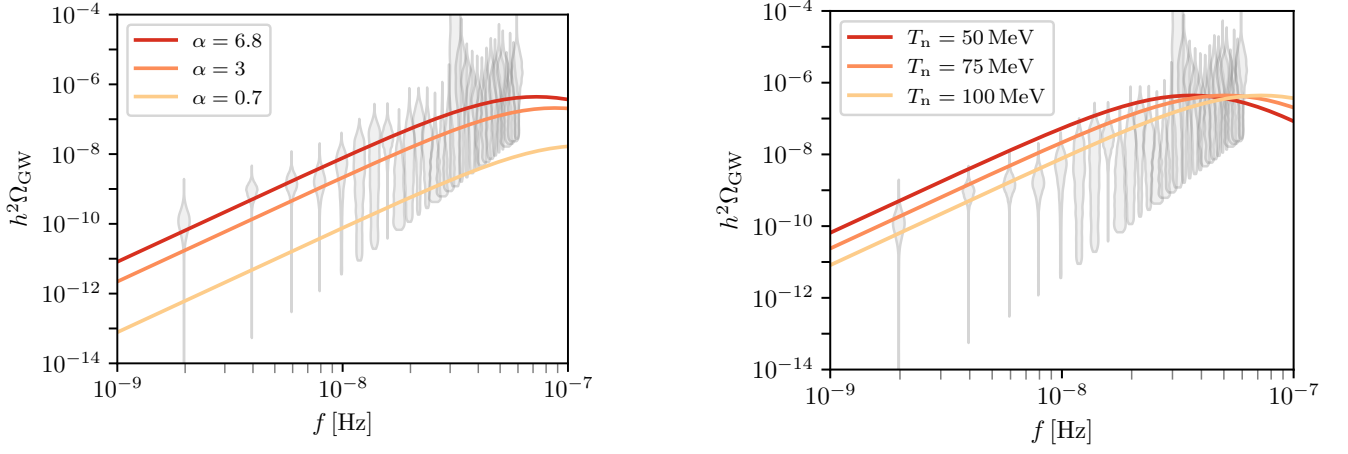


FIG. 2. Gravitational wave spectra from a dilaton-induced QCD PT overlaid with NANOGrav 15-year free-spectrum constraints (gray violins). **Left:** Spectra for transitions at fixed temperature 100 MeV with varying strength, $\alpha = 0.7, 3, 6.8$. **Right:** Spectra for fixed strength $\alpha = 6.8$ and varying temperature, $T_n = 50, 75, 100$ MeV.

given by

$$f_{\text{SW}} = \frac{17.53 \text{ nHz}}{v_w} \frac{\beta}{H_*} \frac{T_n}{100 \text{ MeV}} \left(\frac{g_*}{61.75} \right)^{1/6}. \quad (8)$$

Thus, the dilaton-induced first-order QCD PT proposed in this work results in peak frequencies in the $\mathcal{O}(10\text{--}100 \text{ nHz})$ range.

The corresponding GW energy spectra, $h^2 \Omega_{\text{GW}}$, give the fractional energy density per logarithmic frequency interval, rescaled by the squared Hubble parameter. The GW spectrum from sound waves is then

$$h^2 \Omega_{\text{SW}}(f) = 3.11 \times 10^{-6} \left(\frac{H_*}{\beta} \right) \left(\frac{\kappa_v \alpha}{1+\alpha} \right)^2 \times \left(\frac{61.75}{g_*(T_*)} \right)^{1/3} v_w \left(\frac{f}{f_{\text{SW}}} \right)^3 \left(\frac{7}{4+3(f/f_{\text{SW}})^2} \right)^{7/2}, \quad (9)$$

where the efficiency factor κ_v has been inferred from simulations of ultra-relativistic walls [64], $\kappa_v = \alpha/(0.73 + \alpha + 0.083\sqrt{\alpha})$. We note that Eq. (9) is motivated by simulations of detonations with $\alpha \leq 0.67$ [65, 66]; for larger values of α , it provides an often-used extrapolation.

In Fig. 2 we show the GW energy spectrum generated by the dilaton-induced phase transition for several benchmark values of the parameters. In the right panel we vary the transition strength ($\alpha = 0.7, 3$ and 6) and set $T_n = 100$ MeV, while in the left panel the temperature is varied ($T_n = 50$ MeV, 75 MeV and 100 MeV) and $\alpha = 6.8$. The spectra are overlaid with the posterior distributions from the NANOGrav 15-year free-spectrum analysis [4], shown as gray violins. Remarkably, the predictions of our model are broadly compatible with the observed spectrum.

An explicit model — The dilaton-induced QCD PT can be realised in a range of models. Here, we consider

one simple, explicit example, for concreteness. We defer the construction of an ultraviolet completion of this model to future work. We start from the Lagrangian

$$\mathcal{L} \supset \Lambda_1^2 \frac{\partial_\mu \varphi \partial^\mu \varphi}{2\varphi^2} - \frac{\varphi}{2\Lambda} \text{tr} G_{\mu\nu} G^{\mu\nu}, \quad (10)$$

for the energy scales Λ_1 and Λ . This general form of the Lagrangian, with non-canonical kinetic terms and a linear dependence of the gauge kinetic function on φ , is often found in the four-dimensional supergravity description of string compactifications, where it is common for moduli fields to have logarithmic Kähler potentials and linear holomorphic gauge kinetic functions at tree level.

In terms of the canonically normalised dilaton field, $\phi = \Lambda_1 \ln(\varphi/\Lambda)$, the Lagrangian is given by

$$\mathcal{L} \supset \frac{1}{2} \partial_\mu \phi \partial^\mu \phi - \frac{e^{\phi/\Lambda_1}}{2} \text{tr} G_{\mu\nu} G^{\mu\nu}, \quad (11)$$

i.e., with $\mathbf{f} = \exp(\phi/\Lambda_1)$.

An exponential hierarchy between $\Lambda_{\text{QCD}}^{\text{TV}}$ and $\Lambda_{\text{QCD}}^{\text{FV}}$ is generated if $8\pi^2 \Delta \mathbf{f} / \beta_0 \gtrsim \mathcal{O}(1)$, which gives

$$\frac{8\pi^2}{\beta_0} \Delta \phi f'_{\text{TV}} = \frac{8\pi^2 \mathbf{f}_{\text{TV}}}{\beta_0} \frac{\Delta \phi}{\Lambda_1} \gtrsim \mathcal{O}(1),$$

where we have Taylor expanded \mathbf{f} to leading order. For $\mathbf{f}_{\text{TV}} = 4.2$ this gives a weak lower bound on the separation of the vacua: $\Delta \phi / \Lambda_1 \gtrsim 3 \cdot 10^{-2}$. We assume a toy-model effective potential for ϕ given by

$$V_0(\phi) = \frac{m^2}{2\Delta\phi^2} (\phi - \phi_{\text{TV}})^2 (\phi_{\text{FV}} - \phi)^2 + \frac{\epsilon(\phi - \phi_{\text{FV}})}{\Delta\phi} + V_{\text{np}}(\phi), \quad (12)$$

for which we treat $\phi_{\text{TV}}, \phi_{\text{FV}}, m^2$ and ϵ as free parameters. Note that $\Delta\phi = \phi_{\text{FV}} - \phi_{\text{TV}}$, and $m_{\text{TV/FV}}^2 = m^2$.

The term V_{np} includes contributions that become important for small field values, including the contribution $\sim f_\pi^4(\phi)$ from the linear sigma model, the gluon condensate $\sim -\frac{\beta_0}{32}\Lambda_{\text{QCD}}^4(\phi)$ [67], and further non-perturbative contributions of the form $\sim ce^{-8\pi^2 f(\phi)/\beta_0}$. The potential V_{np} is necessary to ensure that the minimum of the two-field potential $V_{\text{tot}}(\phi, \chi)$ is located at $(\phi_{\text{TV}}, f_\pi^{\text{SM}})$. Finally, we denote as $\Delta V \equiv \epsilon + V_{\text{np}}(\phi_{\text{FV}}) - V_{\text{np}}(\phi_{\text{TV}})$.

To realise the hierarchy of Eq. (7) with a nucleation temperature of $T_n = 100 \text{ MeV}$ one may, for example, choose $m \sim 10 \text{ TeV}$, $\Delta\phi \simeq 2 \times 10^{-3} \text{ GeV}$, $\Delta\phi/\Lambda_1 \sim \mathcal{O}(1)$ and $\Delta V \simeq 0.7\rho_{\text{rad}}(T = 100 \text{ MeV})$. In this case the barrier height in ϕ direction is large, and the thin-wall approximation can be used to estimate S_4 and the decay rate. Thus, our scenario can be realised with a rather minimal set of ingredients.

Discussion — We have shown that quantum tunnelling of the QCD dilaton can turn the QCD phase transition first order and generate a gravitational wave signal intriguingly similar to that observed by Pulsar Timing Arrays.

Our theory can be probed by collider experiments. Dilatons produced through gluon fusion can be searched for through dijet resonances. Data from Run 2 of the Large Hadron Collider (LHC) has already been used to constrain the theory up to $m_\phi \sim 5 \text{ TeV}$ [21]. Data from LHC Run 3, the planned High-Luminosity LHC, and future collider experiments at higher energy will probe some of our theory’s most interesting parameter space.

A first-order QCD PT may source inhomogeneities in the plasma at the onset of Big Bang Nucleosynthesis (BBN), which can affect the abundances of heavy elements [68, 69] (see also [70]). We expect to explore the impact of our dilaton-induced QCD PT on BBN in future work.

An interesting extension of our theory includes the axion, which can be regarded as the pseudo-scalar partner of the dilaton. The mass of the axion increases exponentially from the false vacuum to the true, and an ambient ‘seed’ abundance of axions can be trapped in relic pockets of the false vacuum state [18] (see also [36, 71]). If Δf is sufficiently large, such ‘axion relic pockets’ can be stable and may inherit a substantial fraction of the energy density, ΔV , leading to an overclosure of the universe unless $\alpha \ll 1$. For moderate Δf , the axion relic pockets are transient ‘droplets’, and provide an novel source of small-scale isocurvature.

A further extension of this theory includes an axion-like particle (ALP) coupled to a dark sector confining gauge theory in addition to QCD (i.e. a ‘QCD ALP’ [72]). Such theories often suffer from a problem where stable cosmic domain walls come to dominate the energy density, in conflict with observations. Drawing on the findings of [73, 74], we note that this problem may be solved if the combined ALP and dilaton tunnelling

‘eats’ the domain walls, which may be achieved in theories where $f(\phi)$ is non-monotonic. We expect to make this mechanism more explicit in future work.

Finally, while the explicit model presented in this work illustrates how it may be realised with rather simple ingredients, it would be interesting to embed this toy model in a more complete theoretical framework.

Acknowledgments—We thank Mark Hindmarsh and Filippo Sala for stimulating discussions. This work was supported by the Swedish Research Council (VR) under grants 2018-03641, 2019-02337 and 2024-04289. This article is based upon work from COST Action COSMIC WISPerS CA21106, supported by COST (European Cooperation in Science and Technology).

* aleksandr.chatrchyan@su.se

† david.marsh@fysik.su.se

‡ charalampos.nikolis@fysik.su.se

- [1] J. R. Klauder, ed., *Magic without magic - John Archibald Wheeler. A collection of essays in honor of his 60th birthday.* (Freeman, San Francisco, 1972).
- [2] A. Linde, Particle physics and inflationary cosmology (2005), arXiv:hep-th/0503203 [hep-th].
- [3] Given that the transition is a smooth cross-over, there is no sharply defined critical temperature, but proxies based on e.g. the peak of the disconnected chiral susceptibility have been devised to define the cross-over temperature.
- [4] G. Agazie *et al.* (NANOGrav), The NANOGrav 15 yr Data Set: Evidence for a Gravitational-wave Background, *Astrophys. J. Lett.* **951**, L8 (2023), arXiv:2306.16213 [astro-ph.HE].
- [5] J. Antoniadis *et al.* (EPTA, InPTA:), The second data release from the European Pulsar Timing Array - III. Search for gravitational wave signals, *Astron. Astrophys.* **678**, A50 (2023), arXiv:2306.16214 [astro-ph.HE].
- [6] D. J. Reardon *et al.*, Search for an Isotropic Gravitational-wave Background with the Parkes Pulsar Timing Array, *Astrophys. J. Lett.* **951**, L6 (2023), arXiv:2306.16215 [astro-ph.HE].
- [7] H. Xu *et al.*, Searching for the Nano-Hertz Stochastic Gravitational Wave Background with the Chinese Pulsar Timing Array Data Release I, *Res. Astron. Astrophys.* **23**, 075024 (2023), arXiv:2306.16216 [astro-ph.HE].
- [8] L. McAllister and F. Quevedo, Moduli stabilization in string theory (2023), arXiv:2310.20559 [hep-th].
- [9] L. E. Ibanez and A. M. Uranga, *String theory and particle physics: An introduction to string phenomenology* (Cambridge University Press, 2012).
- [10] V. Kaplunovsky and J. Louis, On gauge couplings in string theory, *Nuclear Physics B* **444**, 191–244 (1995).
- [11] M. Dine and N. Seiberg, Nonrenormalization Theorems in Superstring Theory, *Phys. Rev. Lett.* **57**, 2625 (1986).
- [12] S. Weinberg, Nonrenormalization theorems in nonrenormalizable theories, *Phys. Rev. Lett.* **80**, 3702 (1998), arXiv:hep-th/9803099.
- [13] I. Garcia Garcia, S. Krippendorff, and J. March-Russell, *The String Soundscape at Gravitational Wave Detectors*,

- Phys. Lett. B **779**, 348 (2018), arXiv:1607.06813 [hep-ph].
- [14] B. von Harling and G. Servant, Qcd-induced electroweak phase transition, *Journal of High Energy Physics* **2018**, 10.1007/jhep01(2018)159 (2018).
- [15] S. Ipek and T. M. P. Tait, Early Cosmological Period of QCD Confinement, *Phys. Rev. Lett.* **122**, 112001 (2019), arXiv:1811.00559 [hep-ph].
- [16] D. Croon, J. N. Howard, S. Ipek, and T. M. P. Tait, QCD baryogenesis, *Phys. Rev. D* **101**, 055042 (2020), arXiv:1911.01432 [hep-ph].
- [17] J. Berger, A. J. Long, and J. Turner, Phase of confined electroweak force in the early universe, *Physical Review D* **100**, 10.1103/physrevd.100.055005 (2019).
- [18] P. Carenza, J. Eby, O. Iarygina, and M. C. D. Marsh, Axion relic pockets—a theory of dark matter, *Journal of High Energy Physics* **2024**, 23 (2024).
- [19] F. Gao, S. Sun, and G. White, A first-order deconfinement phase transition in the early universe and gravitational waves (2024), arXiv:2405.00490 [hep-ph].
- [20] I. Bhalla-Ladd, I. Ginnett, and T. M. P. Tait, Leptogenesis during an era of early su(2) confinement (2025), arXiv:2503.09723 [hep-ph].
- [21] U. Danielsson, R. Enberg, G. Ingelman, and T. Mandal, Varying gauge couplings and collider phenomenology, *Phys. Rev. D* **100**, 055028 (2019), arXiv:1905.11314 [hep-ph].
- [22] S. Navas *et al.* (Particle Data Group), Review of particle physics, *Phys. Rev. D* **110**, 030001 (2024).
- [23] J. I. Kapusta and C. Gale, *Finite-temperature field theory: Principles and applications*, Cambridge Monographs on Mathematical Physics (Cambridge University Press, 2011).
- [24] O. Scavenius, A. Dumitru, E. S. Fraga, J. T. Lenaghan, and A. D. Jackson, First order chiral phase transition in high-energy collisions: Can nucleation prevent spinodal decomposition?, *Phys. Rev. D* **63**, 116003 (2001), arXiv:hep-ph/0009171.
- [25] S. P. Klevansky, The nambu—jona-lasinio model of quantum chromodynamics, *Rev. Mod. Phys.* **64**, 649 (1992).
- [26] B.-J. Schaefer, J. M. Pawłowski, and J. Wambach, The Phase Structure of the Polyakov–Quark-Meson Model, *Phys. Rev. D* **76**, 074023 (2007), arXiv:0704.3234 [hep-ph].
- [27] M. Quiros, Finite temperature field theory and phase transitions (1999), arXiv:hep-ph/9901312 [hep-ph].
- [28] M. Laine and A. Vuorinen, *Basics of Thermal Field Theory: A Tutorial on Perturbative Computations* (Springer International Publishing, 2016).
- [29] This correction is valid for the ϕ values we are interested in at temperatures higher than the confinement scale, since the RG-evolved coupling satisfies $\alpha_s(\phi_{TV}, \mu = T) < 1$, so that QCD is still perturbative.
- [30] We note that the interactions of dilaton fluctuations with the gluons with vertex structure $\sim (p_1^\mu p_2^\nu - g^{\mu\nu})$ renormalise the couplings but do not have finite contributions at $T \neq 0$ that could change the shape of the 1-loop thermal potential, and hence we neglect these contributions.
- [31] S. R. Coleman, The Fate of the False Vacuum. 1. Semi-classical Theory, *Phys. Rev. D* **15**, 2929 (1977), [Erratum: *Phys.Rev.D* **16**, 1248 (1977)].
- [32] C. G. Callan, Jr. and S. R. Coleman, The Fate of the False Vacuum. 2. First Quantum Corrections, *Phys. Rev. D* **16**, 1762 (1977).
- [33] N. Barbieri, T. Brinckmann, S. Gariazzo, M. Lattanzi, S. Pastor, and O. Pisanti, Current constraints on cosmological scenarios with very low reheating temperatures, arXiv preprint (2025), arXiv:2501.01369 [astro-ph.CO].
- [34] K. Freese and M. W. Winkler, Have pulsar timing arrays detected the hot big bang: Gravitational waves from strong first order phase transitions in the early universe, *Physical Review D* **106**, 10.1103/physrevd.106.103523 (2022).
- [35] See Supplemental Material for the calculation of the bubble wall velocity and discussion related to the gravitational wave spectrum from runaway bubbles, which includes Refs. [4, 34, 59, 61, 62, 75–94].
- [36] E. Witten, Cosmic Separation of Phases, *Phys. Rev. D* **30**, 272 (1984).
- [37] C. Hogan, Gravitational radiation from cosmological phase transitions, *Monthly Notices of the Royal Astronomical Society* **218**, 629 (1986).
- [38] Z. Arzoumanian *et al.* (NANOGrav), The NANOGrav 12.5 yr Data Set: Search for an Isotropic Stochastic Gravitational-wave Background, *Astrophys. J. Lett.* **905**, L34 (2020), arXiv:2009.04496 [astro-ph.HE].
- [39] H. Middleton, A. Sesana, S. Chen, A. Vecchio, W. Del Pozzo, and P. A. Rosado, Massive black hole binary systems and the nanograv 12.5 yr results, *Monthly Notices of the Royal Astronomical Society: Letters* **502**, L99 (2021).
- [40] D. Izquierdo-Villalba, A. Sesana, S. Bonoli, and M. Colpi, Massive black hole evolution models confronting the n-hz amplitude of the stochastic gravitational wave background, *Monthly Notices of the Royal Astronomical Society* **509**, 3488 (2022).
- [41] A. Afzal *et al.* (NANOGrav), The NANOGrav 15 yr Data Set: Search for Signals from New Physics, *Astrophys. J. Lett.* **951**, L11 (2023), [Erratum: *Astrophys.J.Lett.* **971**, L27 (2024), Erratum: *Astrophys.J.* **971**, L27 (2024)], arXiv:2306.16219 [astro-ph.HE].
- [42] J. Antoniadis *et al.* (EPTA, InPTA), The second data release from the European Pulsar Timing Array - IV. Implications for massive black holes, dark matter, and the early Universe, *Astron. Astrophys.* **685**, A94 (2024), arXiv:2306.16227 [astro-ph.CO].
- [43] T. Bringmann, P. F. Depta, T. Konstandin, K. Schmidt-Hoberg, and C. Tasillo, Does nanograv observe a dark sector phase transition? (2023), arXiv:2306.09411 [astro-ph.CO].
- [44] D. G. Figueroa, M. Pieroni, A. Ricciardone, and P. Simakachorn, Cosmological Background Interpretation of Pulsar Timing Array Data, *Phys. Rev. Lett.* **132**, 171002 (2024), arXiv:2307.02399 [astro-ph.CO].
- [45] J. Ellis, M. Fairbairn, G. Franciolini, G. Hütsi, A. Iovino, M. Lewicki, M. Raidal, J. Urrutia, V. Vaskonen, and H. Veermäe, What is the source of the PTA GW signal?, *Phys. Rev. D* **109**, 023522 (2024), arXiv:2308.08546 [astro-ph.CO].
- [46] A. Addazi, Y.-F. Cai, A. Marciano, and L. Visinelli, Have pulsar timing array methods detected a cosmological phase transition?, *Phys. Rev. D* **109**, 015028 (2024), arXiv:2306.17205 [astro-ph.CO].
- [47] A. Salvio, Supercooling in radiative symmetry breaking: theory extensions, gravitational wave detection and primordial black holes, *Journal of Cosmology and Astroparticle Physics* **2023** (12), 046.
- [48] K. Fujikura, S. Girmohanta, Y. Nakai, and M. Suzuki,

- Nanograv signal from a dark conformal phase transition (2023), arXiv:2306.17086 [hep-ph].
- [49] P. Athron, A. Fowlie, C.-T. Lu, L. Morris, L. Wu, Y. Wu, and Z. Xu, Can supercooled phase transitions explain the gravitational wave background observed by pulsar timing arrays?, *Phys. Rev. Lett.* **132**, 221001 (2024).
 - [50] A. Salvio, Pulsar timing arrays and primordial black holes from a supercooled phase transition, *Physics Letters B* **852**, 138639 (2024).
 - [51] M. W. Winkler and K. Freese, Origin of the stochastic gravitational wave background: First-order phase transition versus black hole mergers, *Phys. Rev. D* **111**, 083509 (2025), arXiv:2401.13729 [astro-ph.CO].
 - [52] K. Fujikura, S. Girmohanta, Y. Nakai, and Z. Zhang, Cold darkogenesis: Dark matter and baryon asymmetry in light of the pta signal, *Physics Letters B* **858**, 139045 (2024).
 - [53] Z.-C. Chen, S.-L. Li, P. Wu, and H. Yu, Nanograv hints for first-order confinement-deconfinement phase transition in different qcd-matter scenarios, *Physical Review D* **109**, 10.1103/physrevd.109.043022 (2024).
 - [54] J. Gonçalves, D. Marfatia, A. P. Morais, and R. Pasechnik, Supercooled phase transitions in conformal dark sectors explain nanograv data (2025), arXiv:2501.11619 [hep-ph].
 - [55] S. Balan, T. Bringmann, F. Kahlhoefer, J. Matuszak, and C. Tasillo, Sub-gev dark matter and nano-hertz gravitational waves from a classically conformal dark sector (2025), arXiv:2502.19478 [hep-ph].
 - [56] A. Brandenburg, E. Clarke, Y. He, and T. Kahnashvili, Can we observe the QCD phase transition-generated gravitational waves through pulsar timing arrays?, *Phys. Rev. D* **104**, 043513 (2021), arXiv:2102.12428 [astro-ph.CO].
 - [57] M. Hindmarsh, S. J. Huber, K. Rummukainen, and D. J. Weir, Gravitational waves from the sound of a first order phase transition, *Phys. Rev. Lett.* **112**, 041301 (2014), arXiv:1304.2433 [hep-ph].
 - [58] M. Hindmarsh, S. J. Huber, K. Rummukainen, and D. J. Weir, Numerical simulations of acoustically generated gravitational waves at a first order phase transition, *Phys. Rev. D* **92**, 123009 (2015), arXiv:1504.03291 [astro-ph.CO].
 - [59] C. Caprini, M. Hindmarsh, S. Huber, T. Konstandin, J. Kozaczuk, G. Nardini, J. M. No, A. Petiteau, P. Schwaller, G. Servant, and D. J. Weir, Science with the space-based interferometer elisa. ii: gravitational waves from cosmological phase transitions, *Journal of Cosmology and Astroparticle Physics* **2016** (04), 001–001.
 - [60] M. Hindmarsh, S. J. Huber, K. Rummukainen, and D. J. Weir, Shape of the acoustic gravitational wave power spectrum from a first order phase transition, *Phys. Rev. D* **96**, 103520 (2017), [Erratum: *Phys. Rev. D* **101**, 089902 (2020)], arXiv:1704.05871 [astro-ph.CO].
 - [61] C. Caprini and D. G. Figueroa, Cosmological Backgrounds of Gravitational Waves, *Class. Quant. Grav.* **35**, 163001 (2018), arXiv:1801.04268 [astro-ph.CO].
 - [62] C. Caprini, M. Chala, G. C. Dorsch, M. Hindmarsh, S. J. Huber, T. Konstandin, J. Kozaczuk, G. Nardini, J. M. No, K. Rummukainen, P. Schwaller, G. Servant, A. Tranberg, and D. J. Weir, Detecting gravitational waves from cosmological phase transitions with lisa: an update, *Journal of Cosmology and Astroparticle Physics* **2020** (03), 024–024.
 - [63] M. B. Hindmarsh, M. Lüben, J. Lumma, and M. Pauly, Phase transitions in the early universe, *SciPost Phys. Lect. Notes* **24**, 1 (2021), arXiv:2008.09136 [astro-ph.CO].
 - [64] J. R. Espinosa, T. Konstandin, J. M. No, and G. Servant, Energy budget of cosmological first-order phase transitions, *Journal of Cosmology and Astroparticle Physics* **2010** (06), 028–028.
 - [65] J. Correia, M. Hindmarsh, K. Rummukainen, and D. J. Weir, Gravitational waves from strong first order phase transitions, arXiv preprint (2025), arXiv:2505.17824 [astro-ph.CO].
 - [66] C. Caprini, R. Jinno, T. Konstandin, A. R. Pol, H. Rubira, and I. Stomberg, Gravitational waves from first-order phase transitions: from weak to strong (2025), arXiv:2409.03651 [gr-qc].
 - [67] M. Shifman, A. Vainshtein, and V. Zakharov, Qcd and resonance physics. theoretical foundations, *Nuclear Physics B* **147**, 385 (1979).
 - [68] J. H. Applegate and C. J. Hogan, Relics of cosmic quark condensation, *Phys. Rev. D* **31**, 3037 (1985).
 - [69] J. H. Applegate, C. J. Hogan, and R. J. Scherrer, Cosmological Baryon Diffusion and Nucleosynthesis, *Phys. Rev. D* **35**, 1151 (1987).
 - [70] H. Bagherian, M. Ekhterachian, and S. Stelzl, The bearable inhomogeneity of the baryon asymmetry (2025), arXiv:2505.15904 [hep-ph].
 - [71] M. Hindmarsh, Axions and the QCD phase transition, *Phys. Rev. D* **45**, 1130 (1992).
 - [72] A. Lella, E. Ravensburg, P. Carena, and M. C. D. Marsh, Supernova limits on QCD axionlike particles, *Phys. Rev. D* **110**, 043019 (2024), arXiv:2405.00153 [hep-ph].
 - [73] S. Blasi and A. Mariotti, Domain walls seeding the electroweak phase transition, *Physical Review Letters* **129**, 10.1103/physrevlett.129.261303 (2022).
 - [74] S. Blasi, A. Mariotti, A. Rase, and A. Sevrin, Axionic domain walls at pulsar timing arrays: Qcd bias and particle friction (2023), arXiv:2306.17830 [hep-ph].
 - [75] P. Schwaller, Gravitational waves from a dark phase transition, *Physical Review Letters* **115**, 10.1103/physrevlett.115.181101 (2015).
 - [76] M. Ahmadvand and K. Bitaghsir Fadafan, The cosmic qcd phase transition with dense matter and its gravitational waves from holography, *Physics Letters B* **779**, 1–8 (2018).
 - [77] I. Baldes, Y. Gouttenoire, and F. Sala, String fragmentation in supercooled confinement and implications for dark matter, *Journal of High Energy Physics* **2021**, 10.1007/jhep04(2021)278 (2021).
 - [78] F. Bigazzi, A. Caddeo, T. Canneti, and A. L. Cotrone, Bubble wall velocity at strong coupling, *Journal of High Energy Physics* **2021**, 10.1007/jhep08(2021)090 (2021).
 - [79] Y. Bea, J. Casalderey-Solana, T. Giannakopoulos, D. Mateos, M. Sanchez-Garitaonandia, and M. Zilhão, Bubble wall velocity from holography, *Phys. Rev. D* **104**, L121903 (2021).
 - [80] M. Sanchez-Garitaonandia and J. van de Vis, Prediction of the bubble wall velocity for a large jump in degrees of freedom, *Phys. Rev. D* **110**, 023509 (2024).
 - [81] E. Morgante, N. Ramberg, and P. Schwaller, Gravitational waves from dark su(3) yang-mills theory, *Physical Review D* **107**, 10.1103/physrevd.107.036010 (2023).
 - [82] X. Han and G. Shao, Stochastic gravitational waves pro-

- duced by the first-order qcd phase transition (2023), arXiv:2312.00571 [astro-ph.CO].
- [83] S. He, L. Li, S. Wang, and S.-J. Wang, Constraints on holographic qcd phase transitions from pta observations, *Science China Physics, Mechanics & Astronomy* **68**, 10.1007/s11433-024-2468-x (2024).
 - [84] J. Shao, H. Mao, and M. Huang, Transition rate and gravitational wave spectrum from first-order qcd phase transitions, *Physical Review D* **111**, 10.1103/physrevd.111.023052 (2025).
 - [85] H. wen Zheng, F. Gao, L. Bian, S. xue Qin, and Y. xin Liu, A quantitative analysis of gravitational wave spectrum sourced from first-order chiral phase transition of qcd (2025), arXiv:2407.03795 [hep-ph].
 - [86] J. M. Cline and B. Laurent, Bubble wall velocity for first-order qcd phase transition (2025), arXiv:2502.12321 [hep-ph].
 - [87] P. Agrawal, G. R. Kane, V. Loladze, and M. Reig, Supercooled confinement (2025), arXiv:2504.00199 [hep-ph].
 - [88] W.-Y. Ai, B. Laurent, and J. van de Vis, Bounds on the bubble wall velocity, *Journal of High Energy Physics* **2025**, 10.1007/jhep02(2025)119 (2025).
 - [89] D. Bödeker and G. D. Moore, Can electroweak bubble walls run away?, *Journal of Cosmology and Astroparticle Physics* **2009** (05), 009–009.
 - [90] Y. Gouttenoire, R. Jinno, and F. Sala, Friction pressure on relativistic bubble walls, *Journal of High Energy Physics* **2022**, 10.1007/jhep05(2022)004 (2022).
 - [91] D. Bödeker and G. D. Moore, Electroweak bubble wall speed limit, *Journal of Cosmology and Astroparticle Physics* **2017** (05), 025–025.
 - [92] A. Kosowsky, M. S. Turner, and R. Watkins, Gravitational waves from first order cosmological phase transitions, *Phys. Rev. Lett.* **69**, 2026 (1992).
 - [93] A. Kosowsky and M. S. Turner, Gravitational radiation from colliding vacuum bubbles: envelope approximation to many bubble collisions, *Phys. Rev. D* **47**, 4372 (1993), arXiv:astro-ph/9211004.
 - [94] S. J. Huber and T. Konstandin, Gravitational wave production by collisions: more bubbles, *Journal of Cosmology and Astroparticle Physics* **2008** (09), 022.
 - [95] A more accurate description of friction in a confinement phase transition is given in [90], and results in the scaling $\mathcal{P}_{\text{friction}} = \mathcal{P}_{\text{BS}} \sim \sum_{i \in \text{BS}} \frac{m_i^2 T_n^2}{24}$, which coincides with that of [89], used here.
 - [96] Another potential friction source is bound state formation from string fragmentation [77]. However, due to insignificant supercooling, we expect confinement to happen among quark pairs rather than quarks forming flux-tubes attached to the bubble wall, and string fragmentation to be unimportant. Even in this scenario though, the leading and next-to-leading order friction from gluons has similar dependence on γ .

Supplemental Material

Bubble wall velocity

In this section, we calculate the pressure exerted on the wall by the quark gluon plasma and determine the terminal speed of the bubble walls. Recall that we consider percolating phase transitions with time-independent Γ . The β -parameter is given by $\beta = \dot{I}(t_*)$, with $I(t)$ the average number of bubbles in the past comoving light cone [34], i.e.

$$\beta = \frac{4\pi\Gamma}{a(t_*)} \int_0^{t_*} dt' a^3(t') r_{\text{com}}^2(t', t_*) , \quad (\text{S013})$$

where $a(t)$ denotes the scale factor, $r_{\text{com}}(t_*, t)$ the comoving bubble radius and t_* the percolation time, defined by $I(t_*) = 1$. As mentioned in the main text, for transitions that percolate, $0 < \alpha \lesssim 20$, which corresponds to $8 \gtrsim \beta/H_* > 3$

The bubble wall velocity is determined by the balance of the driving pressure, $\mathcal{P}_{\text{dr}} \equiv \Delta V$, and the pressure caused by friction from the surrounding plasma, \mathcal{P}_{fr} . The calculation of bubble wall velocities in confining, first-order PTs is an active area of research [75–87]. In this work, the driving pressure is generated by the dilaton potential instead of the confinement dynamics. The expanding bubbles are in the ballistic limit, meaning that the particles in the plasma do not interact significantly over the width of the wall, which in the plasma frame is given by $L_w/\gamma_w \sim 1/(m_\phi\gamma_w)$ where γ_w the Lorentz factor of the wall. The ballistic limit holds when $L_w/\gamma_w \ll L_{\text{MFP}}$, where L_{MFP} is the mean-free path of the particles in the quark-gluon plasma outside the bubbles [88]. Parametrically, we expect $L_{\text{MFP}}^{-1} \sim \alpha_s^2(\phi_{\text{FV}}) T_n$ from $2 \rightarrow 2$ scatterings. Since QCD remains perturbative in the false vacuum, the ballistic approximation holds for all values of γ_w .

The dilaton bubble walls quickly accelerate to ultra-relativistic velocities. Indeed, assuming that quarks and gluons gain masses $\Delta m_q \sim \Delta m_g \sim \Lambda_{\text{QCD}}$ when passing from the deconfined into the confined phase, the ballistic ‘one-to-one’ pressure ($\mathcal{P}_{1 \rightarrow 1}$) from particles passing through or being reflected off the wall was calculated in [88] and reduces to the form of [89] in the ultrarelativistic limit,

$$\mathcal{P}_{1 \rightarrow 1} = \frac{T_n^2}{48} (g_q^* \Delta m_q^2 + 2g_g^* \Delta m_g^2) < \alpha \rho_{\text{rad}} = \mathcal{P}_{\text{dr}} , \quad (\text{S014})$$

where g_q^* , g_g^* denote, respectively, the effective degrees of freedom for quarks and gluons in the plasma. The inequality assumes $\alpha \gtrsim 3 \cdot 10^{-3} (\Lambda_{\text{QCD}}/T_n)^2$, which holds across the most relevant parameter space. Thus, one-to-one processes alone do not suffice to stop the runaway behaviour [89] [95].

Gluon radiation is an additional source of friction. Here, we model the pressure from gluon emission at the wall interface by the equivalent expression for W and Z boson emission when entering bubbles of the low-temperature phase in models where the electroweak PT is first order [91] (we explore an alternative scenario with runaway walls in the next section). Adopting the results of [62, 91], the gluon emission pressure is given by

$$\mathcal{P}_{1 \rightarrow 2} \simeq N_g \Delta m_g \gamma \alpha_s(\phi_w) T_n^3 , \quad (\text{S015})$$

with ϕ_w a value of the dilaton on the wall and $N_g = 8$ is the number of gluons. Here, we have assumed that QCD remains perturbative at the wall, i.e. for an intermediate value of ϕ . This is typically justified since $\Lambda_{\text{QCD}}(\phi_w) \ll \Lambda_{\text{QCD}}^{\text{TV}}$. The pressure contribution $\mathcal{P}_{1 \rightarrow 2}$ grows with γ and eventually catches up with ΔV , leading to an ultra-relativistic terminal velocity with gamma factor [96]

$$\gamma_t = \frac{\Delta V - \mathcal{P}_{1 \rightarrow 1}}{\alpha_s(\phi_w) N_g \Delta m_g T_n^3} \approx 85 \alpha \left(\frac{0.03}{\alpha_s(\phi_w)} \right) \left(\frac{T_n}{\Lambda_{\text{QCD}}} \right) . \quad (\text{S016})$$

By comparing the size of the bubbles when reaching the terminal velocity to their separation β^{-1} , it is clear that the terminal velocity is reached well before bubbles collide.

Gravitational waves from runaway walls

In the main text, we have discussed the GW spectra in the well-motivated scenario where the dilaton bubble walls reach a terminal velocity before colliding. It is instructive to explore the alternate scenario in which the bubble walls

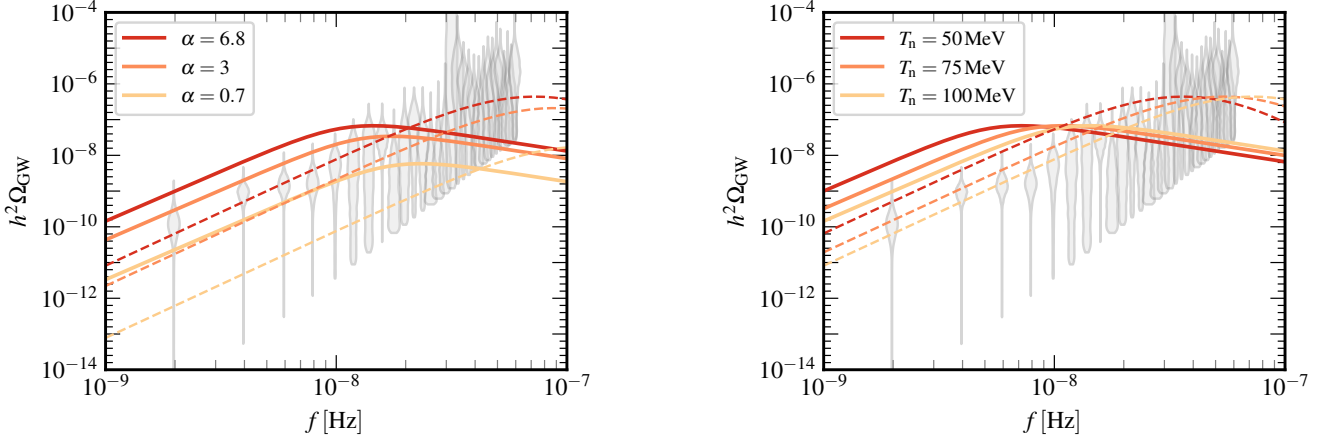


FIG. S1. Gravitational wave spectra from a dilaton-induced QCD PT overlaid with NANOGrav 15-year free-spectrum constraints (gray violins), including the contribution from bubble wall collisions. Solid lines show the spectra in the regime where the energy is carried by bubble walls, while dashed lines correspond to the regime where the energy is converted into sound waves, for comparison. **Left:** Spectra for transitions at fixed temperature 100 MeV with varying strength, $\alpha = 0.7, 3, 6.8$. **Right:** Spectra for fixed strength $\alpha = 6.8$ and varying temperature, $T_n = 50, 75, 100$ MeV.

‘run away’. Such a scenario can be realised in models that yield sufficiently small QCD coupling at the bubble wall interface along with large values of β/H_* so that bubbles never reach their terminal velocity before collision. When this happens, the dominant contribution to the gravitational wave spectrum is given by bubble wall collisions. As discussed in the main text, quantum phase transitions with $\Gamma \simeq \text{constant}$ yield $\beta/H_* \lesssim 8$, which is not very large. However, if the dilaton phase transition is for some reason driven by thermal fluctuations, larger values of β/H_* can be attained, triggering runaway behaviour.

The contribution to the GW signal from bubble wall collisions is dominant if the walls do not convert much of their energy into the surrounding plasma. The GW spectrum in this case can be calculated using the envelope approximation [92–94], where it is assumed that only the uncollided regions of the expanding bubble walls contribute to the energy-momentum tensor [59, 61],

$$h^2\Omega_{\text{coll.}}(f) = 1.96 \times 10^{-5} \left(\frac{H_*}{\beta}\right)^2 \left(\frac{\kappa_{\text{coll.}}\alpha}{1+\alpha}\right)^2 \left(\frac{61.75}{g_*(T_*)}\right)^{1/3} \left(\frac{0.11v_w^3}{0.42+v_w^2}\right) \left(\frac{3.8(f/f_{\text{coll.}})^{2.8}}{1+2.8(f/f_{\text{coll.}})^{3.8}}\right),$$

with peak frequency given by [59]

$$f_{\text{coll}} = \left(\frac{9.44 \text{ nHz}}{1.8 - 0.1v_w + v_w^2}\right) \frac{\beta}{H_*} \frac{T_n}{100 \text{ MeV}} \left(\frac{g_*}{61.75}\right)^{1/6}. \quad (\text{S017})$$

Here $v_w = 1$ and κ_{coll} is energy fraction that is converted into bubble walls. The corresponding spectra are shown in Fig. S1, where we use several benchmark values of the parameters. In the right panel we vary the transition strength ($\alpha = 0.7, 3$ and 6) and set $T_n = 100$ MeV, while in the left panel the temperature is varied ($T_n = 50$ MeV, 75 MeV and 100 MeV) and $\alpha = 6.8$. The spectra are overlaid with the posterior distributions from the NANOGrav 15-year free-spectrum analysis [4], shown as gray violins. For solid lines we assume that all of the energy is in the form of colliding bubble walls, i.e. $\kappa_{\text{coll}} = 1$. The dashed lines in Fig. S1 show the corresponding spectra arising from sound waves, which were discussed in the main text.